Nigerian Journal of Physics (NJP)
ISSN online: 3027-0936
ISSN print: 1595-0611
DOI: 4https://doi.org/10.62292/njp.v33i4.2024.308
Volume 33(4), December 2024

Investigation of the Electrochemical Properties of 3D Recyclable Aluminium doped $LiMn_2O_4$ Electrode: Improved Power and Energy Densities for Lithium-ion Battery Usage

Matthew, A., Jaafar, M., Shalangwa, H. and Muhammad, M.

Department of Physics, Faculty of Natural and Applied Sciences, Nigerian Army University, P.O. Box 1500 Biu, Borno, Nigeria.

*Corresponding author's email: alphamatthew4@gmail.com

ABSTRACT

The Composites of Al-Doped $LiMn_2O_4$; $Al_{0.1}:(LiMn_2O_4)_{0.9}$ and $AI_{0.3}:(LiMn_2O_4)_{0.7,}$ were prepared using the hydrothermal method and drop casting deposition technique. The electrochemical performance of the Al-doped $LiMn_2O_4$ composite as a promising anode material for lithium-ion batteries was characterised by cyclic voltammetry analysis, electrochemical impedance spectroscopy and galvanostatic charge discharge analysis. The anodes' material exhibits a reversible capacity loss, which can be primarily linked to reverse reactions within the solid electrolyte interface formation, aluminium adsorption in the conducting $LiMn_2O_4$, and the electrolyte's electrochemical breakdown. The charges that are retained in the anode material during charging showed a linear decline in charge capacity as charging current intensity increased. Ionic polarisation was the reason for the observed drop in the charge and discharge capabilities at the current density of 5 A/g. Having greater specific capacitance and energy density, the composite $Al_{0.1}:(LiMn_2O_4)_{0.9,}$ is a better anode material for electrochemical applications compared to $Al_{0.3}:(LiMn_2O_4)_{0.7}$, also its comparatively higher power density at a scan rate of 5 mV/s is mostly explained by its lower equivalent series resistance.

Keywords:
Power Density,
Energy Density,
Battery,
Anode,
Electrode.

INTRODUCTION

Lithium-ion battery (LIB) technology is thought to be in development. However, they must perform better for contemporary applications in order to achieve high columbic efficiency, increase power and energy densities. The materials used and the production processes have a significant impact on the ultimate cost of a LIB (Ali *et al*., 2022; Adesina, *et al*., 2021; Kumar, *et al*., 2019; Shichen *et al*., 2023). It is necessary to note that in this industrial period there has seen a sharp rise in the need for energy. Due to their low cost, light weight, and ease of storage, fossil fuels; first carbon, then oil, and finally natural gas have been systematically exploited to power cities and factories (Chen *et al*., 2019; Ahmad *et al*., 2016; Zhao *et al*., 2020; Zhang, *et al*., 2019). But these sources also release a lot of toxic chemicals, such as carbon monoxide, sulphur dioxide, and different nitrogen oxides, making them unfriendly to the environment (Wang *et al.*, 2020). The energy sector has seen new trends and opportunities brought about by the lithium-ion battery, particularly in the burgeoning electric car market. Lithium-ion batteries need to be continuously improved in terms of capacity, power output, life cycle, and safety in order to meet the demands of such applications (Yan *et al*., 2020; Singh *et al*., 2021; Zhang *et al*., 2019). One way to improve these characteristics is to create a more effective and excellent anode electrode material (Diantoro *et al*., 2024; Zhang *et al*., 2020).

This work is aimed at synthesising and investigating the electrochemical properties of aluminium doped $LiMn_2O_4$ as an alternative anode material in LIBs which could be more sustainable and have reduced production costs compare to other graphitic materials.

The specific capacitance (Csp) was evaluated from the equation:

$$C_{sp} = \frac{S}{2mk(E)} \quad (1)$$

S in (mA.V); m in (g); K in mv/s ; and E in (V).

According to Alpha *et al.* (2019) and Zhang, *et al.* (2020), the energy density (E_D) and power density (P_D) were calculated using Equations (2) and (3)

$$E_D = \frac{1}{4} C_{sp} V^2 \quad (2)$$

$$P_D = \frac{V2}{4 \times (ESR)m} \quad (3)$$

MATERIALS AND METHODS

Materials

The chemicals used in this study were of analytical grade with a percentage purity in the range of 99.892 % - 99.999 %. Presented in Table 1 are the lists of chemicals used as precursor materials

Table 1: List of chemicals used as precursor materials

Chemicals	Chemical formula	Manufacturer (Company)	Purity
Lithium manganese IV oxide	$LiMn_2O_4$	Merck	99.995 %
Aluminium Carbonate	$Al_2(CO_3)_3$	Merck	99.995 %
Polyvinylidene fluoride	$-(CH_2=CF_2)_n-$	Merck	99.892 %
Ethanol	CH_3CH_2OH	Merck	99.995 %
N-methyl-2-pyrrolidone (NMP)	C_5H_9NO	Merck	99.999 %
De-ionized water	H_2O	-	99.995 %
Distilled water	H_2O	-	99.995 %

Method

Synthesis Al doped $LiMn_2O_4$ Composites

20 g of the $LiMn_2O_4$ powder, 0.1 mol/L aluminium carbonate solution were added to 1000 ml of distilled water and then stirred using a magnetic stirrer for 3 hours to obtain a composite, $Al_{0.1}:(LiMn_2O_4)_{0.9}$. The composite was then filtered, after which the mixture was sonicated at 78.8 ^oC for 3 hours. After sonication, the sample was then washed with ethanol and dried in an electrical oven at 75 ^oC for 3 hours. The composite, $Al_{0.1}:(LiMn_2O_4)_{0.9}$, was then grinded into a fine powder using a piston and mortar. Also, another 20 g of $LiMn_2O_4$ powder, 0.3 mol/L aluminium carbonate solution were added to 1000 ml of distilled water, and then stirred using a magnetic stirrer for 3 hours to obtain a composite, $Al_{0.3}:(LiMn_2O_4)_{0.7}$. The composite was then filtered, after which the mixture was sonicated at 78.8 ^oC for 3 hours. After sonication, the composite was then washed with ethanol and dried in an electrical oven at 75 ^oC for 3 hours. The composite, $Al_{0.3}:(LiMn_2O_4)_{0.7}$, was then grinded into a fine powder using a piston and mortar.

Preparation of Composites for Characterisation

In the preparation of the composite material for characterisation, a stainless-steel substrate was used. The substrate was first smoothened after which it was washed with distilled water. The substrate was then soaked in an acetone for 1 hour before washing again with distilled water, after which it was ultrasonicated for 30 minutes and then dried in an electric oven for 1 hour. The electrode material was prepared using the drop casting method of deposition. 90 % sample provide, 10 % polyvinylidene fluoride (PVDF) binder were dissolved in N-methyl-2-pyrrolidone (NMP) solvent and stirred for 5 hours until it formed slurry. It was then loaded uniformly onto the treated stainless-steel substrate. After deposition, it was then dried in an electric oven at 120 ^oC for 5 hours. The electrode is formed and ready for characterisaion.

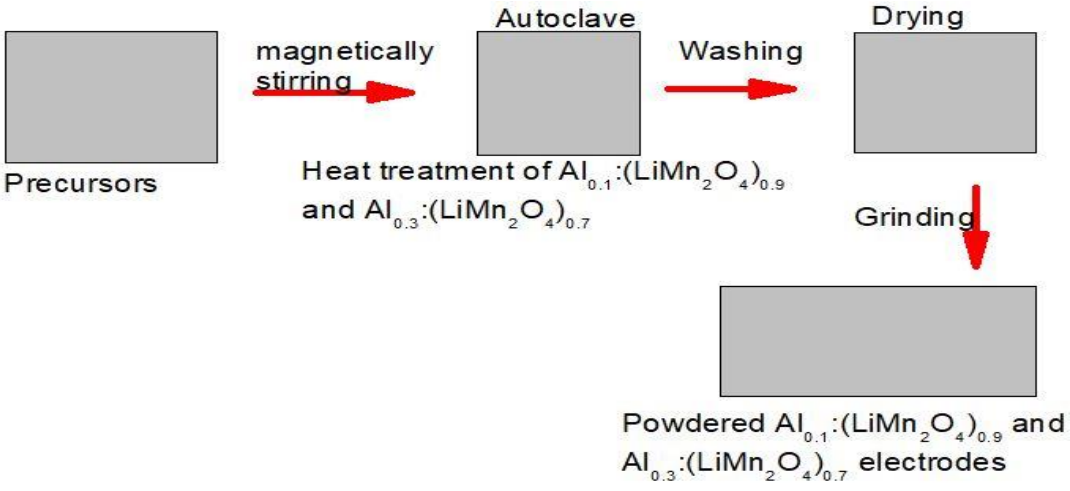

Figure 1: Schematic diagram for the hydrothermal synthesis of $Al_{0.1}:(LiMn_2O_4)_{0.9}$ and $Al_{0.3}:(LiMn_2O_4)_{0.7}$

The electrochemical analysis was carried out in a three electrode configuration with the active material serving as the working electrode, Ag/AgCl serving as the reference through which current flows into the system at a potential window voltage of 0.9 V at a 5 mV/s scan rate and a glassy carbon rod serving as the counter electrode through which the current flows out. A 2 M KOH aqueous solution served as the electrolyte, which provided a medium for current flow and ion interaction, using the electrochemical analyser model CH1604E.

RESULTS AND DISCUSSION

Structural Analysis

X-ray Diffraction (XRD) Analysis for $Al_{0.1}:(LiMn_2O_4)_{0.9}$ and $Al_{0.3}:(LiMn_2O_4)_{0.7}$

Figure 2 shows the stacked crystallites of the XRD pattern for $Al_{0.1}:(LiMn_2O_4)_{0.9}$ and $Al_{0.3}:(LiMn_2O_4)_{0.7}$. This shows the most preferred orientation to be at the diffraction plane (101) (111), and (100) at Bragg's angles of 27.20^0, 25.29^0, and 23.26^0, respectively both composites. This indicated the presence of the crystalline structure of the Al^{3+} and Li^+ in the network of the Mn_2O_4. At higher Bragg's diffraction angles between 30^0 and 70^0, the composites are almost completely amorphous impurities.

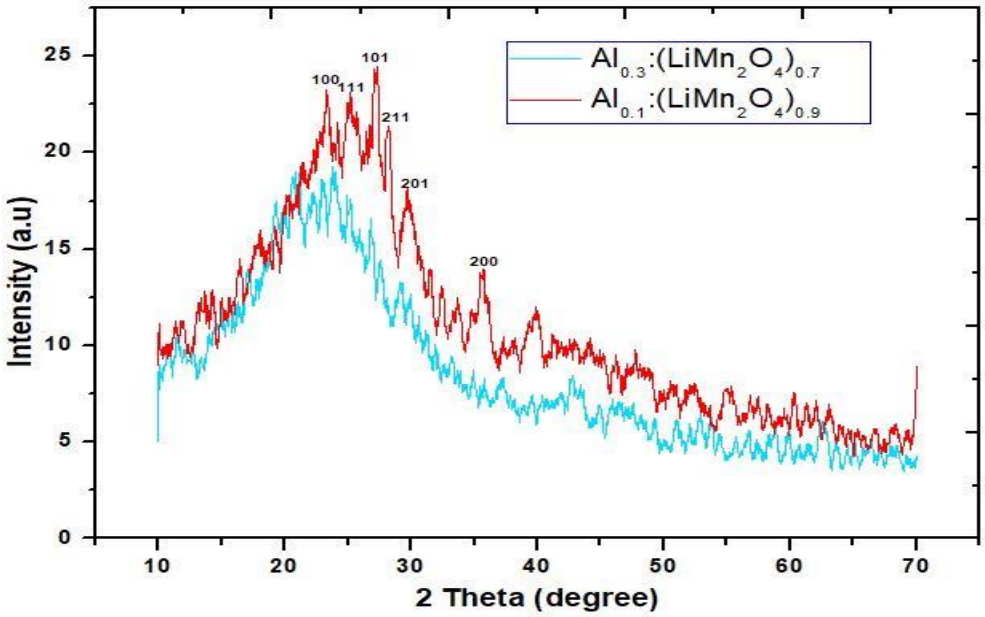

Figure 2: XRD pattern for $Al_{0.1}:(LiMn_2O_4)_{0.9}$ and $Al_{0.3}:(LiMn_2O_4)_{0.7}$

FTIR Spectra Analysis for $Al_{0.1}:(LiMn_2O_4)_{0.9}$ and $Al_{0.3}:(LiMn_2O_4)_{0.7}$

The FTIR spectra for $Al_{0.1}:(LiMn_2O_4)_{0.9}$ and $Al_{0.3}:(LiMn_2O_4)_{0.7}$ were shown in Figure 3.

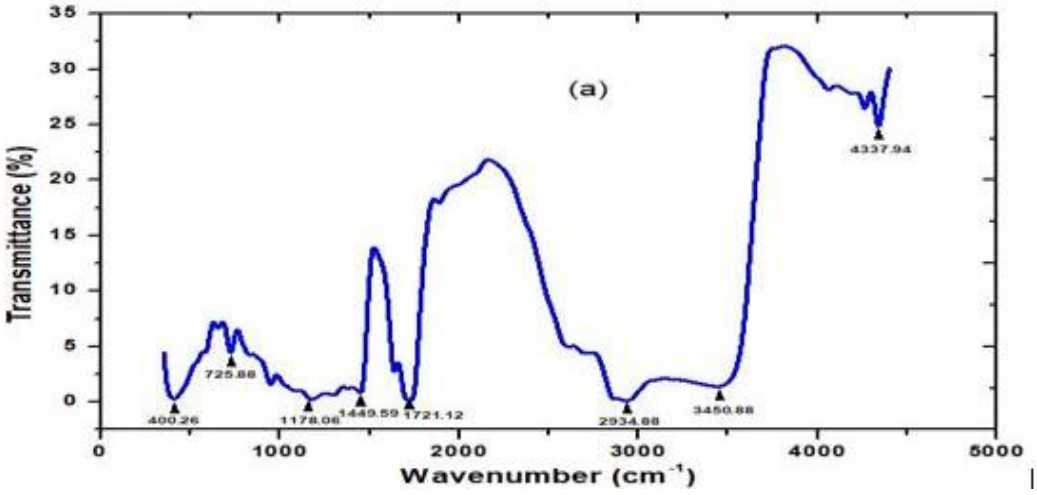

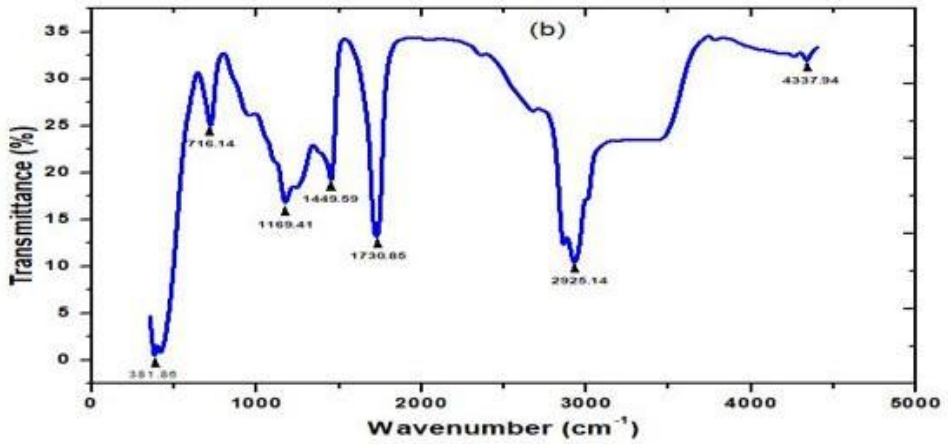

Figure 3: FTIR for (a) $Al_{0.1}$:$(LiMn_2O_4)_{0.9}$ and (b) $Al_{0.3}$:$(LiMn_2O_4)_{0.7}$

The aluminium oxygen functional group was detected in the spectra for both composites between 400 and 1721.12 cm^{-1}, indicating absorption brought on by the bond molecules. This revealed the features of the oxygen molecules' sp^3 vibration, which fall within the group frequency range. At the characteristic peaks, 2934.88 cm^{-1} and 2926.14 cm^{-1}, for $Al_{0.1}$:$(LiMn_2O_4)_{0.9}$ and $Al_{0.3}$:$(LiMn_2O_4)_{0.7}$, receptively, the aluminium oxygen ionic bond was typical at the characteristic peaks, 2934.88 cm^{-1} and 2926.14 cm^{-1}. The structural distortion of the $LiMn_2O_4$ may have been the cause of this change. This might have resulted from the Al ion being introduced into the $LiMn_2O_4$ structure's inter-planner space, which changed the bond distances between the Al, Mn, O, and Li atoms. This structural deformation enhances ionic transport during the electrochemical process.

Electrochemical Analysis

Figure 3 shows the cyclic voltammograms from the cyclic voltammetry analysis for $Al_{0.1}$:$(LiMn_2O_4)_{0.9}$ and $Al_{0.3}$:$(LiMn_2O_4)_{0.7}$ respectively at scan rates of 3 and 5 mVs^{-1}, current density of 100 mA/g. Figures 4 and 5 give the plots for the GCD at 5 A/g for $Al_{0.1}$:$(LiMn_2O_4)_{0.9}$, and $Al_{0.3}$:$(LiMn_2O_4)_{0.7}$. Figures 6 and 7 provide the Nyquist plots from the Electrochemical Impedance Spectroscopy analysis for $Al_{0.1}$:$(LiMn_2O_4)_{0.9}$, and $Al_{0.3}$:$(LiMn_2O_4)_{0.7}$ composites.

Cyclic Voltammetry Analysis

The values of C_{sp}, E_D and P_D were computed using Equations 1, 2, and 3. The summary of the results from the electrochemical analysis for the $Al_{0.1}$:$(LiMn_2O_4)_{0.9}$ and $Al_{0.3}$:$(LiMn_2O_4)_{0.7}$ composite at scan rates of 3 and 5 mVs^{-1} are given in Tables 2 and 3.

Table 2: The Values of C_{SP} and E_D and P_D @ 3mV/s

Composite	Mass (g)	Potential (V)	ERS (Ω)	C_{sp} (F/g)	E_D (Wh/kg)	P_D (kW/kg)
$Al_{0.1}$:$(LiMn_2O_4)_{0.9}$	0.119	1.4	2.0	847.99	115.40	2.059
$Al_{0.3}$:$(LiMn_2O_4)_{0.7}$	0.119	1.4	2.5	484.80	66.00	1.647

Table 3: The Values of C_{SP} and E_D and P_D @ 5mV/s

Composite	Mass (g)	Potential (V)	ERS (Ω)	C_{sp} (F/g)	E_D (Wh/kg)	P_D (kW/kg)
$Al_{0.1}$:$(LiMn_2O_4)_{0.9}$	0.119	1.4	2.0	508.799	53.075	0.349
$Al_{0.3}$:$(LiMn_2O_4)_{0.7}$	0.119	1.4	2.5	353.57	36.7630	0.349

Shown in Figure 4 are the CV curves of the samples acquired at scan rates of 3 and 5 mVs^{-1} between 0.0 and 1.4 V potential window. The insertion or extraction of aluminium from the K $LiMn_2O_4$ lattice was shown to correlate to only one pair of redox peaks. Aluminium is also extremely reversible when it comes to its insertion or extraction from the $LiMn_2O_4$ composite because the CV curves for the cycles are nearly identical. The anode material exhibits a significant reversible capacity loss, which is primarily explained by side reactions including solid electrolyte interface (SEI) formation, aluminium adsorption, and the electrochemical electrolyte breakdown. The composite $Al_{0.1}$:$(LiMn_2O_4)_{0.9}$ at a scan rate of 3 mV/s gives a higher specific capacitance, energy density, and power density, thereby making it a more suitable anode material when used in battery applications this agrees with alpha *et al*. (2019). The composite $Al_{0.1}$:$(LiMn_2O_4)_{0.9}$ at a scan rate of 5 mV/s still maintains a relatively higher power density, this is mainly attributed to its lower equivalent series resistance.

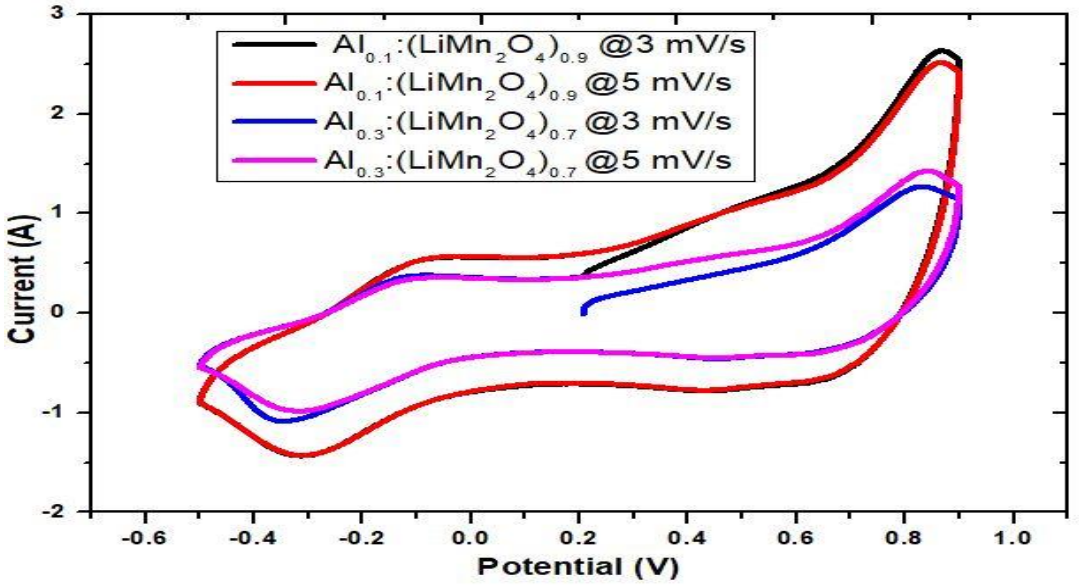

Figure 4: Cyclic Voltamogramm curve at different scan rates for $Al_{0.3}:(LiMn_2O_4)_{0.7}$ and $Al_{0.3}:(LiMn_2O_4)_{0.7}$ composites

GCD Characterisation

The cyclic voltammetry results, which show that redox currents are only set up in this voltage range with an oxidation peak around 0.9 V, demonstrate that the primary cause of the change in the charging voltage is Al^{3+} insertion (the voltage decreases) and extraction (the voltage increases) into and from the $LiMn_2O_4$ anode. High currents indicate rapid changes in the Al ion concentration within the $LiMn_2O_4$ structure's lamellar planes, which in turn implies quick changes in the anode potential over a short amount of time. The values of the specific capacitance and energy densities for $Al_{0.1}:(LiMn_2O_4)_{0.9}$ and $Al_{0.3}:(LiMn_2O_4)_{0.7}$ respectively at current density of 5 A/g for the GCD are shown in Tables 4 and 5. The charge stored in the anode material during charging is represented by a linear reduction in charge capacity with increasing charging current intensity, as seen in Figures 5 and 6.

Table 4: Values of C_{SP} and E_D for $Al_{0.1}:(LiMn_2O_4)_{0.9}$ @5A/g and 1.4 V for GCD

	First cycle	Second cycle	Third cycle	Fourth cycle	Fifth cycle
ΔT	69.15	68.97	68.14	67.91	66.72
ΔV	1.4	1.4	1.4	1.4	1.4
C_{SP}	246.96	246.32	243.34	242.53	238.28
E_D	33.613	33.526	33.121	33.011	32.433

Table 5: Values of C_{SP} and E_D for $Al_{0.3}:(LiMn_2O_4)_{0.7}$ @5A/g and 1.4 V for GCD

	First cycle	Second cycle	Third cycle	Fourth cycle	Fifth cycle
ΔT	23.27	22.39	22.01	21.47	21.39
ΔV	1.4	1.4	1.4	1.4	1.4
C_{SP}	83.107	79.961	78.607	76.678	76.392
E_D	11.311	10.883	10.699	11.436	10.397

The capacitance retention is seen in Figures 6 and 7 for $Al_{0.1}:(LiMn_2O_4)_{0.9}$ and $Al_{0.3}:(LiMn_2O_4)_{0.7}$, having capacity retention of 96.41 % and 91.92 % after five cycles at 5 A/g, respectively.

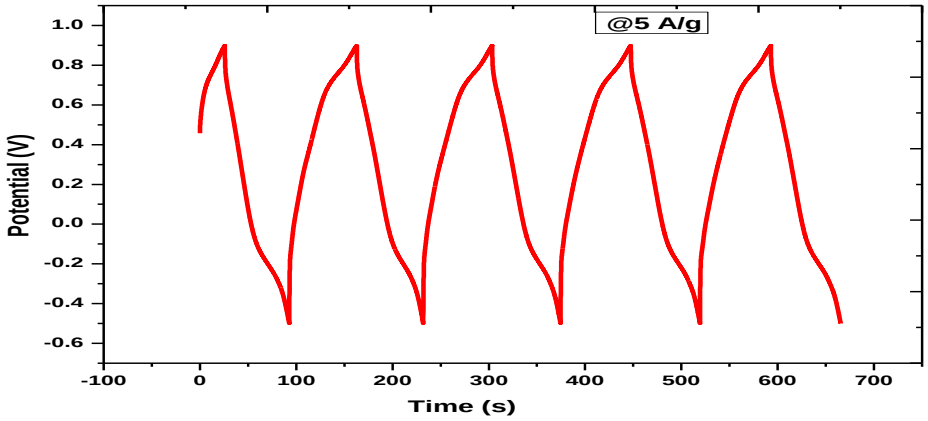

Figure 5: Shows the galvanostatic charge discharge GCD pattern for $Al_{0.1}$:$(LiMn_2O_4)_{0.9}$ composites @ 5A/g

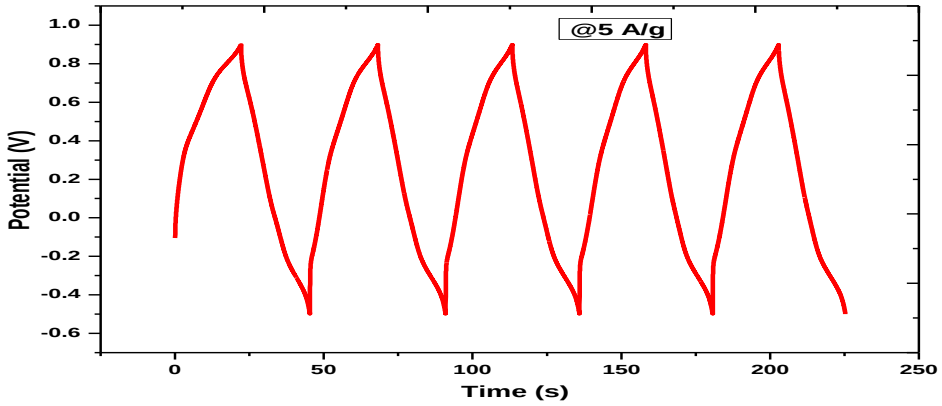

Figure 6: Shows the galvanostatic charge discharge GCD pattern for sample $Al_{0.3}$:$(LiMn_2O_4)_{0.7}$ composites @ 5 A/g

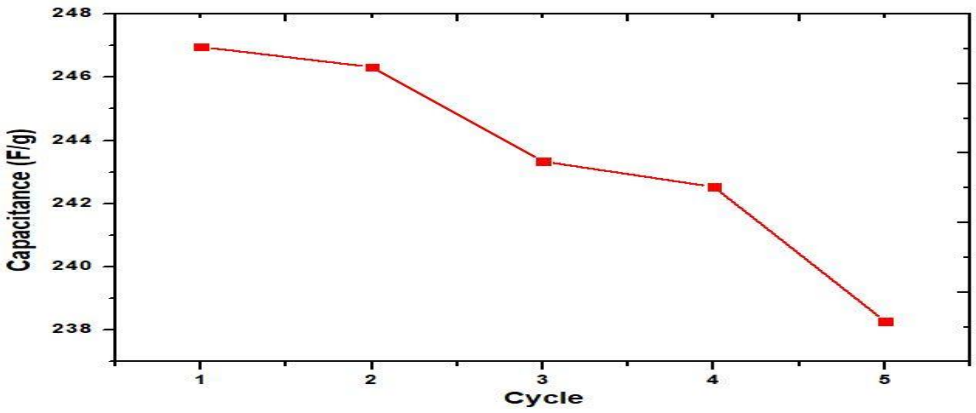

Figure 7: Capacity retention for $Al_{0.1}$:$(LiMn_2O_4)_{0.9}$ composites @5 A/g

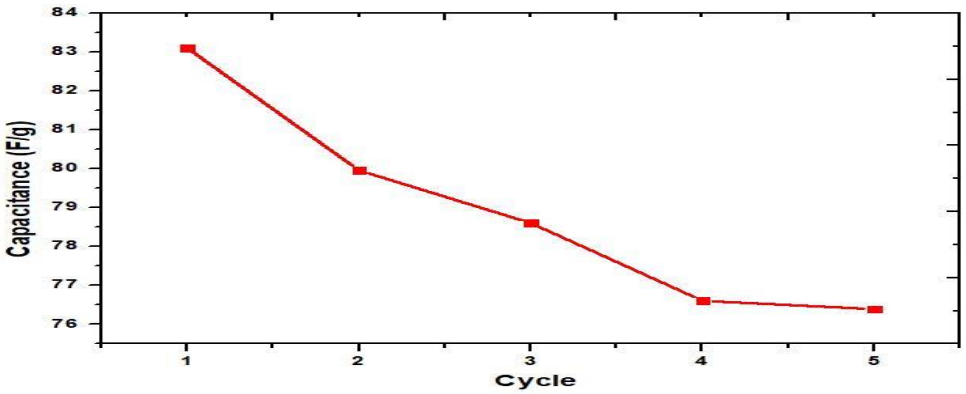

Figure 8: Capacity retention for $Al_{0.3}$:$(LiMn_2O_4)_{0.7}$ composites @5 A/g

EIS Characterisation

In finding out more about the electrochemical properties of the composite anode electrode, EIS measurement was carried out in the frequency range of 100,000 to 0.1 Hz from which the equivalent series resistance (ERS) were estimated. This is seen in Figures 9 and 10.

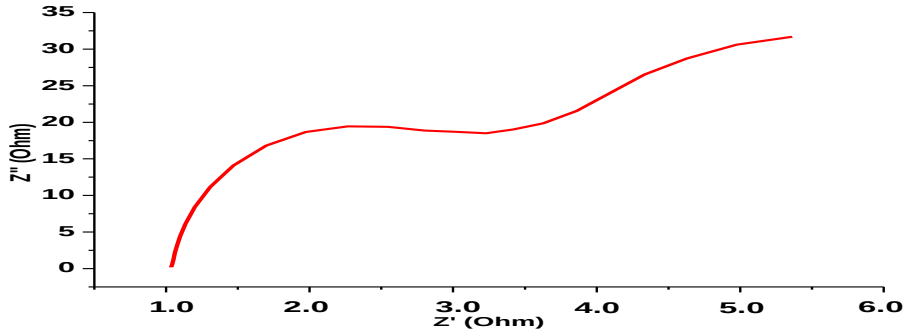

Figure 9: Electrochemical Impedance Spectroscopy Analysis Showing the Nyquist Plot for $Al_{0.1}$:$(LiMn_2O_4)_{0.9}$

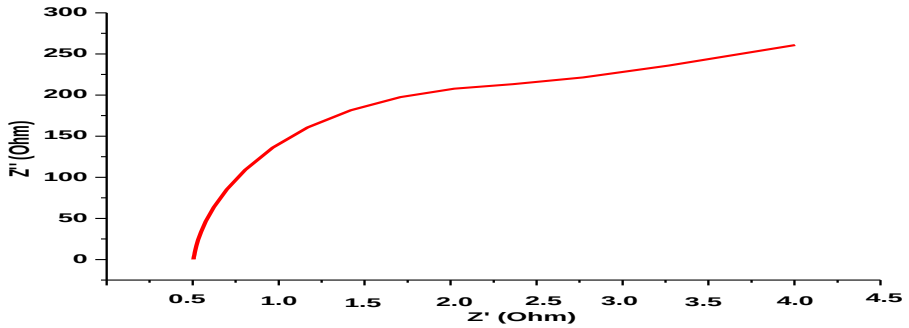

Figure 10: Electrochemical Impedance Spectroscopy Analysis Showing the Nyquist Plot for $Al_{0.3}$:$(LiMn_2O_4)_{0.7}$

CONCLUSION

Al^{3+} was added to the $LiMn_2O_4$ network to enhance charge transfer and ion transport kinetics throughout the composite electrodes. Through the intercalation of cations within the composite material's network, the electrode materials exploited the synergistic advantage. The anodes' material exhibits a reversible capacity loss, which can be primarily linked to reverse reactions within the solid electrolyte interface formation, aluminium adsorption, and the electrolyte's electrochemical breakdown. The charge that is retained in the anode material during charging shows a linear decline in charge capacity as the charging current intensity increases. The observed decrease in charge

and discharge capabilities at the current density of 5 A/g can be explained by ionic polarisation. With a greater specific capacitance and energy density, the composite $Al_{0.1}$:$(LiMn_2O_4)_{0.9}$ is a better anode material for electrochemical applications compared to $Al_{0.3}$:$(LiMn_2O_4)_{0.7}$. The comparatively higher power density of $Al_{0.1}$:$(LiMn_2O_4)_{0.9}$ composite at a scan rate of 5 mV/s is mostly explained by its lower equivalent series resistance.

ACKNOWLEDGEMENT

The research team acknowledges the total financial support/intervention of Tertiary Education Trust Fund (tetfund) 2024, through the Institution Based Research (IBR) grant offer, and the support of the Nigeria Army University Biu for nominating the team for the offer of the tetfund IBR grant.

REFERENCES

Adesina, G.T., Kovo, A.S., and Abdulhamid, M.A. (2021). Effect of Thermal Annealing on the Structural and Electrochemical Properties of Aluminium Doped K_2CO_3 Activated Coconut Husk Carbon-Based Composites. *Journal of Materials Science and Chemical Engineering*, vol. 9, pp. 19-32.

Ali, A., Liang, F., Zhu, J., & Kang, P. (2022). The role of graphene in rechargeable lithium batteries : Synthesis , functionalisation , and perspectives Nano Materials Science The role of graphene in rechargeable lithium batteries : Synthesis , functionalisation , and perspectives. *Nano Materials Science*, *August*. https://doi.org/10.1016/j.nanoms.2022.07.004

Alpha, M., Uno, U.E., Isah, K.U., and Ahmadu, U. (2019). Structural and Electrochemical Properties of Ag_xSnO_{1-x}/G ($0.3 \leq \times \leq 0.4$) Composite Electrode. *European Journal of Scientific Research*, vol. 151, pp. 479-488. http://www.europeanjournalofscientificresearch.com

Ahmad, M.A., Ahmad, N., and Yusoff, A.R. (2016). Potassium hydroxide activated carboderived from coconut husk as a high performance adsorbent for methylene blue. *Ecotoxicology and environmental safety*, vol. 134, pp. 338-345.

Chen, J., Wu, K., Li, W., Chen, K., Cao, D., and Luo, X. (2019). Synthesis of Al_2O_3/K_2CO_3-modified activated carbon derived from coconut husk by microwave-assisted method for high-performance supercapacitors. *Ceramics International*, vol. 45(16), pp. 20476-20486.

Diantoro, M., Rahmadani, H., and Maharani, T. (2024). Microsructure and Electrochemical Performance of Supercapacitor Based on Nickel/Activated Carbon Composite Electrode. *Journal of Physics: Conference Series*, vol. 2734, pp. 01201.

Fangli, Z., Wenchao, Z., David, W., and Zaiping, G. (2022). Recent progress and future advances on aqueous monovalent-ion batteries towards safe and high power energy storage. *Advanced Materials*, vol. 34, 2107965.

Kumar, M., Somanathan, T., and Parthasarathy, S. (2019). Activated carbon from coconut shell as electrode material for supercapacitors, *Journal of Electrochemical Science and Engineering*, vol. 9(2), pp. 103-112.

Lan, H., Qian, S., and Wang, Q. (2017). $Sr_{1-x}Na_{2x}Li_2Ti_6O_{14}$ ($0 \leq x \leq 1$) as anode materials for rechargeable Li-ion batteries. *Ceramics International*, vol. 43, pp. 1552-1557.

Shichen, Y., Yangyang, F., Jing, L., and Yaobing, W. (2023). Metal-Oxide Bicatalysis Batteries for Energy Storage and Chemical Production. *Advanced Materials*, vol. 35(40), pp. 221-227.

Singh, P., Rawat, K.S., Chauhan, D.S., Poddar, P., and Kim, K.H. (2021). Activated coconut husk carbon-based composite for high-performance supercapacitor electrode applications. *Chemical Engineering Journal*, vol. 405, pp. 126937. https://doi.org/10.1016/j.cej.2020.126937

Wang, X., Gao, G., Li, Y., Chen, H., and Ding, X. (2020). Self-healing supercapacitor with high performance based on a hydrogel composite. *Journal of Materials Chemistry A*, vol. 8(6), pp. 3373381, 2020.

Yu, M., Li, R., Wu, M., & Shi, G. (2015). Graphene Materials for Lithium − Sulfur Batteries Graphene materials for lithium – sulfur batteries. *Energy Storage Materials*, *1*(January 2019), 51–73. https://doi.org/10.1016/j.ensm.2015.08.004

Yan, L., Fang, L., Zhang, Y., Hao, X., and Sun, X. (2020). Enhanced Li+ ion transference number of Al-doped K_2CO_3 solid electrolyte via rational design. *Journal of Materials Science:Materials in Electronics*, vol. 31, pp. 7242-7251.

Zhao, H., Xu, Z., Zhang, L., Liu, Y., and Che, F. (2020). Modified coir-based activated carbon for enhanced removal of methylene blue: Preparation, characterization and adsorption properties. *Journal of*

Environmental Chemical Engineering, vol. 8, pp. 104083. https://doi.org/10.1021/acscentsci.0c00449

Zhang, H., Cao, J., Chen, X., Wang, J., Bian, K., and Yuan, H. (2019). Rational design and synthesis of K_2CO_3: Al_2O_3 solid electrolytes with high ionic conductivity for lithium ion batteries. *Journal of Energy Chemistry*, vol. 38, pp. 67-73.

Zhang, H., Bian, K., Yang, W., Wang, J., Li, X., and Yuan, H. (2017). Ionic conductivity improvement of K_2CO_3:Al_2O_3 solid electrolyte with a high Al content for lithium-ion batteries. *Electrochimica Acta*, vol. 238, pp. 246-253.

Zhang, Q., Zhang, B., Ma, S., Wang, R., Zhu, C., and Zhao, X.S. (2020). Preparation and Evaluation of Coconut Shell-Based Activated Carbon with High Performance as Supercapacitor Electrode Materials. *Journal of Energy Storage*, vol. 31, pp. 101651, 2020.